NUCPHA 1675

Search for highly deformed shape isomers in ^{28}Si, ^{24}Mg and ^{20}Ne linked by successive alpha decays.

G. R. Kelly,* N. M. Clarke, M. Freer, B. R. Fulton, S. J. Hoad, R. A. Le Marechal, and R. P. Ward*

School of Physics and Space Research, University of Birmingham, Edgbaston, Birmingham B15 2TT, U.K.

Abstract

Measurements of the $^{12}C(^{16}O,^{20}Ne\ \alpha)\alpha$, $^{12}C(^{16}O,\alpha\ \alpha)^{20}Ne$, $^{12}C(^{16}O,^{8}Be)^{20}Ne$ and $^{12}C(^{16}O,^{16}O\ \alpha)^{8}Be$ reactions have been performed at $E_{c.m.}$ = 27.0 MeV. For decays proceeding through resonant states in the intermediate ^{24}Mg nucleus, angular correlation measurements have enabled spin assignments to be made and the dominant entrance channel angular momentum to be determined. The results are inconsistent with recent similar experiments which were interpreted as arising from successive α–decays from deformed shape isomeric states in ^{28}Si and ^{24}Mg.

PACS numbers: 21. 60. -n, 25. 70. Ef, 25. 70. Gh, 27. 30. +t

KEYWORDS: nuclear reactions, $^{12}C+^{16}O$, $E_{c.m.}$ = 27 MeV, highly deformed shape isomers, sequential alpha decay

Typeset using REVTeX

I. INTRODUCTION

Many nuclear models predict that highly deformed shape isomers exist in light nuclei. In particular, Nilsson-Strutinsky (NS) [1], Hartree-Fock (HF) [2] and Bloch-Brink α-cluster models (ACM) [3] indicate several structures in nuclei ranging from ^{12}C to ^{48}Cr. In a number of cases, the stability of these structures has been explored through the inclusion of a cranking term in the NS [4] or ACM [5] models, indicating that they are capable of supporting a rotational sequence to high angular momentum. Various authors have suggested that rotational bands based on such shape isomers may explain the striking scattering resonances observed in a number of heavy ion systems, for example ^{24}Mg [^{12}C+^{12}C] [6], ^{32}S [^{16}O+^{16}O] [7], ^{48}Cr [^{24}Mg+^{24}Mg] [8] or ^{56}Ni [^{28}Si + ^{28}Si] [9]. However, the models often predict a number of shape isomers in each nucleus, based on different configurations, and it is not clear which structure would be responsible for the resonances, nor indeed whether the resonances should indicate a number of bands based on the different configurations.

The situation is well illustrated by the ^{24}Mg nucleus. In this case, Marsh and Rae performed [5] an unconstrained cranked ACM calculation, in which they identified six different metastable configurations. These authors were able to show a one–to–one correspondence between these configurations and the secondary minima appearing in the ^{24}Mg potential energy surface from the NS and HF calculations. These range from structures with low deformation (comparable to the ^{24}Mg ground state) to those with high deformation (corresponding to a prolate 3:1 deformation). There have been suggestions that some of these structures might correspond to resonances seen in different exit channels in ^{12}C+^{12}C scattering [6], and more recently as the origin of a rotational sequence observed in the breakup of ^{24}Mg $\rightarrow$ ^{12}C + ^{12}C observed in the ^{12}C(^{24}Mg,^{12}C ^{12}C)^{12}C reaction [10]. However, it is difficult to provide a firm association to specific configurations since a number of these have similar moments of inertia, and often the only information available is the E_{ex} versus $J(J+1)$ systematics.

Recently, Eswaran *et al.* [11] suggested that it may be possible to uniquely associate a scattering resonance to a particular shape isomeric configuration by looking at the configuration of the states to which the resonance decayed (an idea used earlier by Ledoux *et al.* [12]). In this work, these authors looked at the decay of a resonance in ^{28}Si observed in ^{12}C+^{16}O scattering at $E_{c.m.}$ = 26.9 MeV. The resonance appeared strongly in a number of exit channels, in particular to states between 7–8 MeV in ^{20}Ne which the authors associated with the 0^+ and 2^+ members of the 0_3^+ band. Moreover, they reported that these members of the 0_3^+ band appeared to be preferentially populated over the ground state 0_1^+ band. Since the 0_3^+ band is believed to be based on an 8p-4h ^{12}C-2α configuration [13,14], the authors suggested that the ^{28}Si resonance was based on a 16p-4h ^{12}C-4α configuration. This allowed them to associate the ^{28}Si resonance with the oblate $(\epsilon,\gamma) = (1.35,60°)$ minimum appearing in the NS calculations. The authors also reported a strong decay to states near 20 MeV excitation in the ^{20}Ne + α channel, which they suggested might be members of a band based on the oblate $(\epsilon,\gamma) = (1.2,60°)$ minimum in ^{24}Mg, which the NS calculations indicate is based on a 12p-4h configuration.

In a follow-up experiment (Kumar *et al.* [15]), the same group explored this latter suggestion by tracing the successive α-decay through a measurement of the ^{12}C(^{16}O,α α)^{20}Ne reaction. They were unable to measure the spin of the ^{24}Mg states, but presented arguments based on penetrability calculations to suggest that they were $J^\pi \sim 8^+$ (and so consistent with the suggested NS 12p-4h association), and also that the successive α-decay again went preferentially to the 0_3^+ band members in ^{20}Ne rather than the ground state band members.

In a comment on the first paper, Zhang *et al.* [16] raised a question about the configuration association. However, a much more serious problem with the interpretation arose with the later results reported by Sugimitsu *et al.* [17] who performed an extensive search for resonant structures in the reaction ^{12}C(^{16}O,^{8}Be)^{20}Ne reaction. This measurement involved wide angular coverage, 21 angles as opposed to the single angle of the original Eswaran *et al.* measurement, and also required unique identification of the ^{8}Be nuclei from the coincident detection of the two decay α–particles, as opposed to simultaneous detection in a single detector as in the original Eswaran *et al.* measurement. The Sugimitsu *et al.* measurement failed to find any resonance at $E_{c.m.} = 26.9$ MeV in any of the ^{8}Be + ^{20}Ne decay channels up to around 9 MeV of excitation in ^{20}Ne (which includes the 0_3^+ band members).

The possibility that sequences of α-decays can be traced between highly deformed minima in neighbouring nuclei, and be used to identify the configuration of these states, is very appealing and offers the potential for important spectroscopic studies. Hence it is important that the validity of this interpretation is checked.

In this paper we report a re-measurement of the ^{12}C(^{16}O,α α)^{20}Ne reaction at $E_{c.m.} = 27.0$ MeV in addition to a measurement of the ^{12}C(^{16}O,^{20}Ne α)α, ^{12}C(^{16}O,^{8}Be)^{20}Ne and ^{12}C(^{16}O,^{16}O α)^{8}Be reactions, performed with large-area, position-sensitive detectors. The greatly improved resolution achieved in this measurement enabled the yields from particular decay sequences to be measured much more accurately. It also enabled angular correlation measurements to be made from which it is possible to extract the spins of most of the intermediate states in ^{24}Mg. The results from the present measurement do not support the interpretation proposed by Eswaran *et al.* and Kumar *et al.*

II. EXPERIMENTAL PROCEDURE AND DATA ANALYSIS

The experiment was performed at the Australian National University 14UD tandem accelerator using an $E_{beam} = 63.0$ MeV ($E_{c.m.} = 27.0$ MeV) $^{16}O^{6+}$ beam to bombard a ^{12}C target of 27μm cm^{-2} areal thickness. The integrated charge during the experiment was 3.29 mC, measured using a Faraday cup at the back of the scattering chamber. Particles were detected using four position–sensitive silicon strip detectors (PSSD). Each of these PSSD's consisted of 16 horizontal silicon strips, of 3 mm pitch and 0.1 mm vertical separation, fabricated on a single silicon wafer of overall area 50$\times$50 mm^2. The front contact on each strip had a resistive layer enabling position information to be obtained by recording the signal taken from either end of each strip. The vertical position of the strip in the PSSD provided the out–of–plane position information for each detected particle.

One of the PSSD's was incorporated within a gas hybrid detector to enable heavy ion particle identification. The centre of the hybrid detector was set at $+14.8°$ relative to the beam, subtending a laboratory angle of $12.9°$. The three other PSSD's, labelled here as PSSD2, PSSD3 and PSSD4, used for detecting α–particles only, were centred at $+39.9°$, $-28.0°$ and $-55.0°$ relative to the beam respectively, each subtending a laboratory angle of $22.6°$. The solid angle covered by the hybrid was 50 msr, and by each of the other PSSD's was 155 msr. Figure 1 shows schematically the setup of the detectors. Only the top eight strips of PSSD3 were used in the present experiment, owing to a faulty electronic module, effectively reducing the solid angle coverage for this PSSD to 77 msr.

The construction and use of the gas hybrid detector is described by Curtis *et al.* [19]. The hybrid used a 3.5 μm aluminised mylar window to contain propane gas at a pressure of 50 torr. This ionisation chamber produced a ΔE signal for each particle passing through it. In later offline analysis, a plot of ΔE versus E produced loci corresponding to different nuclei (with different A and Z). Heavy ions of interest were selected by placing a software window around the corresponding locus.

To enable the maximum number of detectors to be used within the 128 channel capacity of the data acquisition system, the PSSD's were connected in a 'doubled–up' arrangement. In this, pairs of strips from adjacent PSSDs were connected together, producing a total of three signals, one from each end and one from the central mutual connection. These three signals were then sent to three analogue–to–digital converters before being written to data tape. Timing information was also recorded from each pair of doubled–up strips, and sent to 32 timing–to–digital convertors.

III. RESULTS

To analyse a three body final state reaction, it is only necessary to record the energy and scattering angle of two of the final state particles. The energy and angle of the third (unobserved) particle is determined by the requirement that momentum be conserved in the reaction. The experimental setup enabled us to measure the $\alpha + \alpha + {}^{20}$Ne exit channel in two ways, either by identifying the ^{20}Ne in the hybrid in coincidence with an α–particle in one of the strip detectors, or by identifying an α–particle in the hybrid in coincidence with a second α–particle in the strip detectors. By virtue of the detector geometry, the former will probe forward angles for the emission of the intermediate ^{24}Mg* nucleus (typically $0° \leq \Theta_{c.m.} \leq 60°$), while the latter will probe backward angle emission (typically $140° \leq \Theta_{c.m.} \leq 170°$). Since we do not have any particle identification in the strip detectors, there will be some background arising from coincidences with other nuclei. However, as will be seen later in the analysis, this background mostly falls outside the areas of interest in the energy spectra.

The setup also enabled the ^{8}Be + ^{20}Ne exit channel to be investigated by detecting a double α–particle hit in one of the strip detectors and checking that the relative energy of the two α–particles equalled 92 keV, corresponding to the breakup energy of the ^{8}Be ground state. In addition, the ^{12}C(^{16}O,^{16}O α)^{8}Be reaction was also studied by detecting α–particles in coincidence with ^{16}O nuclei in the hybrid.

A. ^{20}Ne + α coincidences

Figure 2 shows the E_{tot} spectrum for the coincident events at where a ^{20}Ne was detected in the hybrid and an α–particle in PSSD3 (a similar spectrum is obtained for coincident α–particles in PSSD4). E_{tot} is a measure of the total kinetic energy in the exit channel – the sum of the measured energy for the ^{20}Ne and α–particle plus the calculated energy of the unobserved α–particle – and hence reflects the Q–value of the reaction. The peak labelled Q_{ggg} corresponds to all three particles emerging in their ground states. Peaks are also observed corresponding to when ^{20}Ne nuclei emerge in the 1.63 MeV (2^+) or 4.25 MeV (4^+) members of the ground state band, or in the 7.00 MeV (4^-) and 10.61 MeV (6^-) members of the 2^- band. Although these latter two are above the α–decay threshold at 4.73 MeV their unnatural parity prohibits α–decay so that the ^{20}Ne nuclei survive to enter the hybrid.

As can be seen, the Q_{ggg} appears not to be clearly resolved from the neighouring peak.

Both peaks also sit upon a background due to random coincidences. When considering events within the Q_{ggg} peak, by placing careful and accurate software gates, the amount of 'feed–through' from the neighbour is seen in the later analysis to be small. This 'feed–through' is, however, still taken into account in the following discussion.

Figures 3(a) and 3(b) show the reconstructed ^{24}Mg excitation spectra for events within the Q_{ggg} peak where the ^{20}Ne nuclei were detected in their ground state in the hybrid detector and α–particles in PSSD3 and PSSD4, respectively. A rich spectrum of states in ^{24}Mg is observed. The lines overlaying each spectrum are the results of Monte Carlo simulations [20] of the detection efficiency. In these, the Monte Carlo calculations simulate the reaction by assuming an isotropic angular distribution for the ^{24}Mg* and subsequent breakup fragments. The breakup fragments are tracked to see whether they hit the detectors, taking into account the effects of energy thresholds and rejecting events where two fragments hit the same strip. Events where two particles were detected in adjacent connected strips were rejected in the offline analysis. This was also accounted for in the Monte Carlo simulations.

The peak centroids and Full–Widths–at–Half–Maximum (FWHM) for each of these spectra are listed in tables I and II. Only the stronger peaks have been considered in order to avoid subjectivity and to ensure the measured peaks do correspond to events within the Q_{ggg} peak. The centroids and FWHM were extracted using the BUFFIT [27] peak fitting code, accounting for the background level and minimizing the χ^2 fit. A maximum systematic error of ± 150 keV was estimated from uncertainties in the detector positions and energy calibrations. The error in the measurement of each centroid is no more than 25 keV. The identification and measurement of some states between 20 and 22 MeV which are listed in table II but not in table I was due to the different phase space coverage between the two detector setups. A good level of agreement is observed between the two tables of results.

In addition, figure 4 shows the reconstructed ^{24}Mg excitation spectra, for events when the breakup occurs to the 1.63 MeV (2^+) or 4.25 MeV (4^+) states in ^{20}Ne. In these spectra, the coincident α–particles were detected in PSSD3.

Information on the spin of the breakup states which α–decay to the ground state in ^{20}Ne can be obtained from the angular correlation of the breakup fragments [21]. Briefly, the angular correlation can be expressed in terms of the centre of mass scattering angle Θ^* of the excited ^{24}Mg nucleus and the breakup angle Ψ, where Ψ is the angle between the relative velocity vector of the two breakup fragments and the beam axis. For the Q_{ggg} events, as both particles in the entrance and exit channels are spin zero, for ^{24}Mg nuclei scattered at Θ^*=0°, only the m=0 sub–state can be populated, where the beam direction is taken as the quantization axis. The distribution of the yield of breakup fragments as a function of Ψ is then represented by the square of a Legendre polynomial of order l. A measure of the periodicity of the yield at Θ^*=0° then identifies the spin of the state. If the excited ^{24}Mg nucleus is scattered away from Θ^*=0°, then the restriction on populating m=0 sub–states is removed and the resulting angular correlation takes the form of a ridge structure in the Θ^*–Ψ plane [21]. By projecting the data back along the ridges onto the Θ^*=0° axis, the spin of the state can be determined by comparing the periodicity, but *not* necessarily the amplitude, of the projected data with Legendre polynomials of various orders.

It has also been shown by da Silveira [22] that, if there is a dominant partial wave in the reaction, the spin of the state is proportional to the gradient of the ridges in the Θ^*–Ψ plane. This follows from the relation

$$\frac{d\Theta^*}{d\Psi} = \frac{J}{l_f} \tag{1}$$

where $l_i = J + l_f$, and l_i and l_f denote the dominant partial waves in the entrance and exit channels, respectively. These angular correlation measurements can, therefore, be used to provide two independent determinations of the spin for the states which α–decay to the ground state in ^{20}Ne. (Further examples of this technique can been seen in, for example, references [23–25]).

For the ^{20}Ne$_{g.s.}$ + α data measured in the hybrid and PSSD3 coincidence measurement, the spin assignments, taken from the periodicity of the projected angular correlations, are listed in table I. Similarly, the data measured in the hybrid and PSSD4 combination are listed in table II. The error in the deduced l_i is due to the error in determining the exact slope (and hence projection angle) of the correlation pattern. In the instances where it was not clear which squared Legendre polynomial best reproduced the data, both spins (i.e. both orders of polynomial) have been tabulated. This, in turn, leads to two possible values for l_i.

Some peaks may be composed of two or more unresolved states. In these instances, one would not be able to assign any possible spins using the technique described above. In addition, if a peak arose because of the 'feed–through' from the neighbouring peak in the E_{tot} spectrum, the non–zero exit channel spin would wash out the angular correlations (because a number of partial waves would contribute). The observation of correlations supports the association of these states, to which spins have been assigned, to the Q_{ggg} exit channel. The ^{20}Ne + α breakup spectrum of ^{24}Mg is well known and the states at lower excitation energies which are observed in the present work have been observed in previous measurements of the same reaction [26]. Within this reference, only those states observed in reactions with *identical* entrance *and* exit channels (labelled by superscripts g, z, β, κ) have been considered. As can be seen, given experimental uncertainties in the measurement of peak centroids, the present and reference data give similar spin assignments for states up to $\sim$17.9 MeV, although it was not possible to assign probable spins for all of the states observed in the present work.

This confirms the validity of the angular correlation approach and since we extract a consistent value for l_i in all cases, this in turn supports the assignments for the two states above 20 MeV whose spins were previously unknown. The state observed at 20.4 MeV excitation has been assigned a probable spin of $J^\pi = 8^+$. The projected correlations for this state and the state at 23.0 MeV (whose spin was also previously unknown) are shown in figure 5. For comparison, the squared Legendre polynomials one order higher and lower than the one that best reproduces the observed correlations are also shown. Only these two projections are shown here, as these are new measurements and are important for the later discussion.

B. $\alpha + \alpha$ coincidences

Figure 6 shows the reconstructed ^{24}Mg excitation spectrum from the α–particles detected in the hybrid detector, from the reaction ^{12}C(^{16}O,α)^{24}Mg, in coincidence with another particle in PSSD2 data (a similar spectrum is obtained for coincidences with PSSD3). The lower energy threshold at $E_{ex}(^{24}Mg)$ ~18 MeV corresponds to where the α–particles are too energetic to be fully stopped by the detector ($E_{lab}(\alpha)$ ~32 MeV). The large background at higher excitation energies may be due to low energy α–particles unrelated to this exit channel.

Figure 6 shows clearly the states at 20.2 and 21.4 MeV seen in the measurements by Eswaran *et al.* and Kumar *et al.* (again with a maximum systematic error of ±150 keV). In addition, another state is observed at 23.4 MeV. By gating on these states in ^{24}Mg, we can use the information from the coincident α–particle to reconstruct the excited states in ^{20}Ne to which these ^{24}Mg states decay. This is shown in figure 6 which shows coincidences between the hybrid and PSSD2 (a similar spectrum is obtained for coincidences between the hybrid and PSSD3). If the rôle of the detected α–particles were reversed, such that the α–particles detected in PSSD2 were associated with the breakup of $^{28}\mathrm{Si} \rightarrow {}^{24}\mathrm{Mg} + \alpha$, then the ~20 MeV states do not appear so clearly. This is due to the lack of particle identification available with this detector.

In this spectrum, a number of peaks in ^{20}Ne can be seen at 0.0, 1.6, 4.3, 5.6, 7.3 and 8.8 MeV. The first of these can be identified unambiguously with the 0^+, 2^+ and 4^+ members of the ground state band. Beyond this, the resolution is not sufficient to associate peaks in the spectrum with specific states in ^{20}Ne. For example the peak at ~5.6 MeV could be the 5.62 MeV (2^-) and/or the 5.79 MeV (1^-) states, while there are five states known in the region of the broad peak at ~7.3 MeV.

In interpreting these spectra, we must also exercise care in a number of other respects. Firstly, the detection efficiency varies with energy, as indicated by the dotted line which is the result of the Monte Carlo simulation as described earlier. Secondly, the reaction energetics are such that the ^{20}Ne states at higher excitation can only be populated from the decay of the higher excited ^{24}Mg states. Of course the cut-off will not be abrupt, but near the threshold, it will be very strongly influenced by penetration through the Coulomb barrier. The procedure of calculating transmission coefficients using the optical model, as performed by Kumar *et al.*, is fraught with uncertainties. There are ambiguities in extracting the optical model parameters by fitting elastic scattering data. By using different potentials from the literature (e.g. [28]), we find that the ratios can vary by an order of magnitude. Also, the elastic scattering data from which the potentials are obtained is measured at much higher energies than the few MeV relevant for the α-decays. These parameters are deduced phenomenologically and it is very unlikely that, determined at one energy, they will be equally valid at a very different energy. In addition, the potentials from the elastic scattering reflect the potential between an α–particle and a ^{20}Ne in the ground state, not in an excited state (and if this is deformed, there is the additional uncertainty of the choice of channel radius for the Coulomb potential). Hence, the yield of states should *not* be interpreted unless well away from these threshold effects. In this respect, the population of the 7–8 MeV states in ^{20}Ne from the decay of the 20.2 and 21.4 MeV ^{24}Mg states cannot be compared with optical model calculations with any reasonable confidence.

Thirdly, there is a background under the peaks in the ^{24}Mg excitation spectrum which may contribute to the ^{20}Ne spectrum. To investigate the extent of this we have gated on equivalent width regions above and below each ^{24}Mg state, evaluated and averaged the two ^{20}Ne spectra for these data, and then subtracted this background yield from the 'on–peak' spectrum. The resulting spectrum, shown in figure 7 may then be regarded as a measure of the *sequential* α-decay of ^{28}Si, through these intermediate ^{24}Mg states, to ^{20}Ne. This reveals that only members of the ground state band survive in the background subtracted yield, with no significant yield to either the ^{20}Ne ground state itself or the 7–8 MeV states. As there is a possibility of unresolved ^{24}Mg states either side of the 20.2, 21.4 and/or 23.4 MeV states affecting this background subtraction procedure, figure 7 should only be considered as an indication of the states populated by the sequential α-decay of ^{28}Si, through ^{24}Mg, to

^{20}Ne. It is, however, gratifying that the relative yields of the decays from each ^{24}Mg state to various states in ^{20}Ne in figure 7 generally complement the intensities of the corresponding decays observed in figures 3 and 4.

C. The ^{8}Be + ^{20}Ne exit channel

By detecting double α–particle hits in strip PSSD3 and PSSD4 we can measure the ^{8}Be + ^{20}Ne channel. For such coincident events, the relative energy of the ^{8}Be is calculated, as shown in figure 8. The clear peak at 92 keV corresponds to the decay of the ^{8}Be ground state into two α–particles. By gating on this peak, we can reconstruct the momentum vector of the initial ^{8}Be nucleus from the two α–particle momenta, and hence record a spectrum of excited states in ^{20}Ne populated in the reaction ^{12}C(^{16}O,^{8}Be)^{20}Ne. This spectrum is shown in figure 9(a) and represents an angle averaged yield over the range $30° \leq \Theta_{c.m.} \leq 110°$ (increasing to 130° for the decays to the higher excited states in ^{20}Ne).

As the ^{20}Ne level density below $\sim$8 MeV excitation is quite low , it is possible to unambiguously associate certain peaks with specfic states in the ^{20}Ne excitation spectrum in this region based just on their centroids and the observation of the complete band to which that state belongs [13].

The spectrum shows the 0^+ (0.00 MeV), 2^+ (1.63 MeV) and 4^+ (4.25 MeV) members of the ground state band, the strength of the peaks increasing with increasing spin. Strong peaks are also observed at 8.8 and 12.0 MeV which probably correspond to the 6^+ (8.77 MeV) and 8^+ (11.98 MeV) band members, although the density of states in ^{20}Ne at these higher excitations is such that other states may also contribute to these peaks. Two other peaks are observed which can also be identified unambiguously; the first is the 2^- (4.97 MeV) state of the 2^- band. The observation of the 2^- state suggests that the other members of this band will be excited (3^-, 5.6 MeV; 4^-, 7.00 MeV; 5^-, 8.45 MeV; 6^- 10.6 MeV and 7^-, 13.34MeV) and indeed there are peaks in the spectrum at energies which would correspond to all of these states, although again it should be noted that other states may also be contributing to these peaks. The second is a small peak observed at 7.8 MeV which can be assigned to the 2^+ (7.81 MeV) member of the 0_3^+ band. The 0_3^+ band head state is at 7.19 MeV and so may contribute (along with the 4^-, 7.00 MeV state) to the peak at $\sim$7 MeV. However, based on how the yields of the ground state and 2^- bands vary with angular momentum, the 0_3^+ (7.19 MeV) yield would be below that of the 2^+ (7.81 MeV) state and hence only a minor part of this peak.

Further information on the states observed in these spectra can be obtained by looking at the ^{16}O + α coincidence data and reconstructing the ^{20}Ne excitation spectrum. These ^{12}C(^{16}O,^{16}O α)^{8}Be events reveal the subsequent α-decay of the excited ^{20}Ne states observed in figure 9(a). This spectrum is shown in figure 9(b). As well as giving a spectrum with much improved resolution, the angular momentum correlation technique can also be used to provide spin assignments. At $E_{c.m.}$ = 27.0 MeV, the angular coverage includes the region around $\Theta^* = 0°$, enabling model independent spin assignments to be made for the four strongest states at 8.79 (6^+), 10.30 (5^-), 12.00 (8^+ or 6^+) and 12.65 MeV (6^+). These assignments are in accord with the results of Rae *et al.* [29] for the same reaction at the much higher beam energy of 150 MeV ($E_{c.m.}$ = 64.3 MeV) where a direct reaction process would be presumed to dominate. The coverage for the state at 7.15 MeV excitation does not include the region $\Theta^* = 0°$ but by projecting at an angle corresponding to the dominant angular momentum indicated by the above four states, the spin is assigned as $J^\pi = 3^-$. This is the 3^- member of the 0^- band, of which the strong state at 10.30 MeV is the 5^- member. In addition, the state at 15.35 MeV is assigned a possible spin of 7^-, which would also identify it as a member of this band. The observation of the 3^- state in this spectrum is important in that it indicates that this state is contributing to the unresolved peak at $\sim$7 MeV in the ^{8}Be + ^{20}Ne coincidence spectrum. Finally, there is a very weak peak at just under 8 MeV which may be the 2^+ member of the 0_3^+ band, but the yield is too small to be certain.

IV. DISCUSSION

From the $\alpha + \alpha$ coincidences in this study we note that the states at 20.2 and 21.4 MeV in ^{24}Mg decay to the ^{20}Ne ground state band members (figure 7). We also note, from the $^{20}\mathrm{Ne}_{g.s.} + \alpha$ coincidence measurements, that in the region $\mathrm{E}_{ex}(^{24}\mathrm{Mg}) \sim 20$ MeV, the spins of the states are around $J^\pi \sim 8^+$. We are also able to assign spin of $J^\pi = 16^+$ to the $\mathrm{E}_{c.m.} = 27.0$ MeV resonance in ^{28}Si (or more correctly, we deduce that the dominant angular momentum in the $^{12}\mathrm{C}+^{16}\mathrm{O}$ collision which leads to the $\alpha + \alpha + {}^{20}\mathrm{Ne}$ channel is $l_i = 16\ \hbar$). These are close to the values $J^\pi \sim 8^+$ assigned by Kumar *et al.* for the 20.2 and 21.4 MeV states in ^{24}Mg on the basis of penetrability arguments and $J^\pi = 14^+$ assigned by Eswaran *et al.* for the resonance in ^{28}Si from the $^{12}\mathrm{C}(^{16}\mathrm{O},\alpha)^{24}\mathrm{Mg}_{g.s.}$ angular distribution at this energy.

However, the $\alpha + \alpha$ coincidence data does not support the assertion by Eswaran *et al.* and Kumar *et al.* that the 20.2 MeV state decays preferentially to the 0_3^+ band members in ^{20}Ne as compared to the ground state band members. This is based on an interpretation of the spectra in figure 7 which shows the states in ^{20}Ne which are fed through the α–decays from the 20.2, 21.4 and 23.4 MeV states in ^{24}Mg. In this background subtracted spectra, there is no evidence for the 0^+ and 2^+ members of the 0_3^+ band. A peak does appear at $\sim$7 MeV in the non–background subtracted spectra, but here the feeding may be from other routes rather than via the specific states in ^{24}Mg, e.g. α–pickup onto the beam, which would also lead to a $^{20}\mathrm{Ne} + \alpha + \alpha$ final state. Eswaran *et al.* and Kumar *et al.* associated a peak at a similar energy seen in their measurement as arising from the 0^+ and 2^+ members of the 0_3^+ band (at 7.2 and 7.8 MeV, respectively). However, there are three other states in this energy region and as we have evidence that at least two of these are excited in this channel (the 4^-, 7.00 MeV state is seen in the $^{20}\mathrm{Ne} + \alpha + \alpha$ E_{tot} spectrum and in the ^{8}Be + ^{20}Ne exit channel, and the 3^-, 7.16 MeV state seen in the $^{16}\mathrm{O} + \alpha$ coincidence data) this association cannot be confirmed. Hence, there is no evidence in the present data that the α–decay of the 20.2 and 21.4 MeV states in ^{24}Mg preferentially populates the 8p-4h states at 7–8 MeV excitation in ^{20}Ne. The possibility that other states could be contributing was not considered by the analyses of Eswaran *et al.* and Kumar *et al.*

The $^8Be + ^{20}Ne$ measurements are also not in accord with the picture suggested by Eswaran *et al.* and Kumar *et al.* The more extensive measurements on the $^{12}C(^{16}O,^8Be)^{20}Ne$ system by Sugimitsu *et al.* have indicated that there does not appear to be a resonance in the $^8Be + ^{20}Ne$ channel at $E_{c.m.} = 27.0$ MeV, and certainly not in the 7–8 MeV states in ^{20}Ne. The present measurement of the $^8Be + ^{20}Ne$ channel also shows no indication for these states being preferentially excited relative to the ground state members. Indeed, a detailed examination of the states populated, using the additional information obtained by studying the subsequent $^{16}O + \alpha$ decay of the excited ^{20}Ne nucleus, shows no evidence for the 0_3^+ state. There is some evidence for the 2^+ band member at 7.83 MeV, but the yield is certainly well below that of the observed ground state band, in contrast with the conclusions of Kumar *et al.* deduced from their analysis. Because of the contributing yield from other states, which was not considered in the analyses of Eswaran *et al.* and Kumar *et al.*, it was not possible to extract a value for the ratio of the 0_3^+:0_1^+ bandheads as it is also not possible to determine the level of the 7.2 MeV (0_3^+) state's contribution to the $\sim$7 MeV peak in figure 9(a).

As a final comment, it is tempting to associate the 20.2, 21.4 and 23.4 MeV states in ^{24}Mg with a $^{20}Ne + \alpha$ cluster configuration due to the survival of just the ^{20}Ne ground state band members in figure 7. However, if these ^{24}Mg states were decaying statisically, one might expect a greater α–decay yield to the higher spin states in ^{20}Ne based on a reduced angular momentum barrier argument (remembering that this is only valid for those ^{20}Ne states well away from Coulomb barrier threshold effects). Consequently, it is not safe to make this suggestion based just on the present study. Direct measurement of the spins of these three ^{24}Mg states would be very useful but this was not possible in the present study due to the lack of any significant α–decay yield to the (spin zero) ^{20}Ne ground state.

V. SUMMARY

A new measurement of the ^{12}C(^{16}O,α α)^{20}Ne reaction has been made using large-area position-sensitive detector telescopes. This has provided much improved data compared with previous measurements. Analysis of these data does not support the suggestion proposed by Eswaran *et al.* and Kumar *et al.* that the resonance at $E_{c.m.}$ = 27.0 MeV decays preferentially through ^{8}Be emission to the 7–8 MeV 0_3^+ states in ^{20}Ne, and via successive α–particle emission to the same states via states in ^{24}Mg at 20.2 and 21.4 MeV. Taken together with the recent measurement by Sugimitsu *et al.* which shows no resonance in the ^{12}C(^{16}O,^{8}Be)^{20}Ne channel at this energy, these results do not support the conjecture by Eswaran *et al.* and Kumar *at al.* that the resonance in ^{28}Si is based on an oblate shape isomer, which in turn is linked to the oblate isomers in ^{24}Mg and ^{20}Ne.

ACKNOWLEDGMENTS

GRK and SJH acknowledge the support of studentships from the Engineering and Physical Sciences Research Council (EPSRC). The experiment was performed under an agreement between the Australian National University (ANU) and EPSRC and the authors thank the staff at the ANU for their help. The authors would also like to thank Dr. W. D. M. Rae for his helpful comments.

REFERENCES

* Present address: School of Sciences, Staffordshire University, College Road, Stoke-on-Trent, ST4 2DE, U.K.

[1] G. Leander and J. E. Larsson, Nucl. Phys. **A 239** (1975) 93.

[2] H. Flocard, P. H. Heenen, S. J. Kreiger and M. S. Weiss, Prog. Theor. Phys. **72** (1984) 1000.

[3] D. M. Brink, Int. School of Physics 'Enrico Fermi' XXXVII (1966) 247.

[4] I. Ragnarsson and Sven Åberg, Physica Scripta **24** (1981) 215.

[5] S. Marsh and W. D. M. Rae, Phys. Lett **180B** (1986) 185.

[6] E. Almqvist, D. A. Bromley and J. A. Keuhner, Phys. Rev. Lett **4** (1960) 515.

[7] B. R. Fulton and W. D. M. Rae, J. Phys.**G 16** (1990) 333.

[8] R. W. Zürmuhle, P. Kutt, R. R. Betts, S. Saini, F. Haas and O. Hansen, Phys. Lett. **129B** (1983) 384.

[9] R. R. Betts, B. B. Back and B. G. Glagola, Phys. Rev. Lett **47** (1981) 23.

[10] N. Curtis, N. M. Clarke, B. R. Fulton, S. J. Hall, M. J. Leddy, A. St. J. Murphy, J. S. Pople, R. P. Ward, W. N. Catford, G. J. Gyapong, S. M. Singer, S. P. G. Chappell, S. P. Fox, C. D. Jones, D. L. Watson, W. D. M. Rae and P. M. Simmons, Phys. Rev. **C 51** (1995) 1554.

[11] M. A. Eswaran, Suresh Kumar, E. T. Mirgule, D. R. Chakrabarty, V. M. Datar, N. L. Ragoowansi and U. K. Pal, Phys. Rev. **C 47** (1993) 1418.

[12] R. J. Ledoux, C. E. Ordonez, M. J. Bechara, H. A. Al-Juwair, G. Lavelle and E. R. Cosman, Phys. Rev. **C 30** (1984) 866.

[13] M. M. Hindi, J H. Thomas, D. C. Radford and P. D. Parker, Phys. Rev. **C 27** (1983)

2902.

[14] R. Middleton, J. D. Garrett and H. T. Fortune, Phys. Rev. Lett. **27** (1971) 950.

[15] Suresh Kumar, M. A. Eswaran, E. T. Mirgule, D. R. Chakrabarty, V. M. Datar, N. L. Ragoowansi, U. K. Pal and H. H. Oza, Phys. Rev. **C 50** (1994) 1535.

[16] J. Zhang, A. C. Merchant and W. D. M. Rae, Phys. Rev. **C 48** (1993) 2117.

[17] T. Sugimitsu, N. Hori, H. Fujita, Y. Funatsu, N. Kato, K. Kimura, M. Matsuo, S. Mitsuoka, T. Mukae, S. Niiya, T. Okamoto, H. Yamaguchi and Y. Nakayima, Nucl. Phys. **A 586** (1995) 190.

[18] M. J. Bechara, A. J. Lazzarini, R. J. Ledoux and E. R. Cosman, Phys. Rev. **C 27** (1983) 1540.

[19] N. Curtis, A. St. J. Murphy, M. J. Leddy, J. S. Pople, N. M. Clarke, M. Freer, B. R. Fulton, S. J. Hall, G. Tungate, R. P. Ward, S. M. Singer, W. N. Catford, G. J. Gyapong, R. A. Cunningham, J. S. Lilley, S. P. G. Chappell, S. P. Fox, C. D. Jones. D. L. Watson, P. M. Simmons, R. A. Hunt, A. C. Merchant, A. E. Smith, W. D. M. Rae and J. Zhang, Nucl. Instr. Methods **351** (1994) 359.

[20] M. Freer, Computer code MAUL (University of Birmingham), unpublished.

[21] S. Marsh and W. D. M. Rae, Phys. Lett. **153B** (1985) 21.

[22] E. F. da Silveira, Proc. 14^{th} Winter Meeting on Nuclear Physics, Bormio, (1976) 293.

[23] W. D. Rae, P. R. Keeling and S. C. Allcock, Phys. Lett. **184B** (1987) 133.

[24] M. Freer, NIMS **A 383** (1996) 463.

[25] M. Freer, N. M. Clarke, R. A. Le Marechal, G. Tungate, R. P. Ward and W. D M. Rae, Phys. Rev. **C 51** (1995) 3174.

[26] R. Abegg and C. A. Davis, Phys. Rev. **C 43** (1991) 2523 and references therein.

[27] N. M. Clarke, Computer code BUFFIT (University of Birmingham), unpublished.

[28] D. Shapira, R. G. Stokstad and D. A. Bromley, Phys. Rev. **C 10** (1974) 1063.

[29] W. D. M. Rae, S. C. Allcock and J. Zhang, Nucl. Phys. **A 568** (1991) 271.

FIGURES

FIG. 1. Schematic diagram showing the arrangement of the detectors relative to the beam.

FIG. 2. The E_{tot} plot for the reaction $^{12}C(^{16}O,^{20}Ne\ \alpha)\alpha$ at E_{beam} = 63 MeV ($E_{c.m.}$ = 27.0 MeV). The Q_{ggg} peak corresponds to all three final state particles emerging from the reaction in their ground states. Other peaks visible correspond to excited states in the ^{20}Ne nucleus.

FIG. 3. Reconstructed excitation spectra for states observed in the $^{12}C(^{16}O,^{20}Ne_{g.s.}\ \alpha)\alpha$ reaction at each beam energy for events detected within (a) the gas hybrid and PSSD3 and (b) the gas hybrid and PSSD4. The efficiency profiles are scaled such that the maximum value on the ordinate in each case corresponds to an absolute efficiency of 2%. The reduction in solid angle coverage of PSSD3 (see text) has been taken into account.

FIG. 4. Reconstructed excitation spectra for states observed in the $^{12}C(^{16}O,^{20}Ne^{*}\ \alpha)\alpha$ reaction at $E_{c.m.}$ = 27.0 MeV for events detected within the gas hybrid and PSSD3. The efficiency profile is scaled such that the maximum value on the ordinate corresponds to an absolute efficiency of 2%.

FIG. 5. The projected angular correlations for the (a) 20.4 and (b) 23.0 MeV states observed in the $^{12}C(^{16}O,^{20}Ne_{g.s.}\ \alpha)\alpha$ reaction. In this instance the coincident α–particles were detected in PSSD4. Similar projections were obtained for coincident α–particles detected in PSSD3. Overlaying each projection is a squared Legendre polynomial. The order of the polynomial is indicated in the top left of each box.

FIG. 6. In the top panel, the ^{24}Mg excitation spectrum deduced from α–particle events within the hybrid. In the lower three panels are ^{20}Ne excitation spectra indicating the population of the states after gating on specific states in ^{24}Mg observed in the upper panel. The efficiency profile is scaled such that the maximum value on the ordinate corresponds to an absolute efficiency of 0.06%.

FIG. 7. As for figure 6, but with a level of background removed indicating the sequential α-decay of ^{28}Si, through specific states in ^{24}Mg, to ^{20}Ne (see text for a description of the background subtraction procedure). The efficiency profile is scaled such that the maximum value on the ordinate corresponds to an absolute efficiency of 0.06%

FIG. 8. An example of the ^{8}Be excitation spectrum deduced from the detecting double α–particle hits in PSSD3 and PSSD4. The clear peak at 92 keV corresponds to the relative energy of the two α–particles following the breakup of the ^{8}Be ground state.

FIG. 9. The reconstructed ^{20}Ne excitation spectra observed in the (a) ^{12}C(^{16}O,^{8}Be)^{20}Ne and (b) ^{12}C(^{16}O,^{16}O α)^{8}Be reactions. The efficiency profile is scaled such that the maximum value on the ordinate corresponds to an absolute efficiency of (a) 0.4% and (b) 2%.

TABLES

TABLE I. Table detailing the centroids and Full-Width-at-Half-Maximum of the states observed in the reaction ^{12}C(^{16}O,^{20}Ne α)α at $E_{c.m}$ = 27.0 MeV. The ^{20}Ne and α are detected in coincidence in the hybrid and PSSD3, respectively. (The assymetric peak near 17.7 MeV has been fitted as an unresolved doublet). Where two possible spin assignments have been suggested, it is not clear which squared Legendre polynomial best reproduced the data. In reference [26], only those states observed through an identical entrance and exit channel to the present work have been considered.

E_{ex}	FWHM	J^π	l_i	ref. [26]	
(MeV)	(keV)	($\hbar$)	($\hbar$)	E_{ex} (MeV)	J^π ($\hbar$)
12.14	239±8				
12.51	156±8	4^+	15.9±0.3	12.49	4^+
13.10	348±23			13.07	5^-
				13.20	4^+
13.48	164±3	$6^+/7^-$	15.9±0.3/18.6±0.3	13.42	6^+
				13.75	5^-
				13.84	6^+
14.17	223±4	6^+	15.9±0.3	14.14	4^++6^++8^+
				14.41	4^+
14.75	242±69	4^+	16.1±0.2		
15.24	244±26			15.13	4^+
				15.15	4^++7^-
16.16	267±18	$7^-/6^+$	16.1±0.1/13.8±0.1	16.07	6^+
				16.30	8^+
				16.46	7^-
16.55	255±7	6^+	16.1±0.2	16.55	8^++9^-
				16.59	6^+
16.97	292±38			16.84	8^+

				16.86	6^+
17.54	169±19	6^+	16.6±0.7	17.60	(6^+)
17.81	341±17	6^+	16.0±0.3	17.9	$(4^+ + 6^+)$
18.66	430±82	$5^-/6^+$	14.1±0.4/16.0±0.4		
19.61	279±25				
20.41	286±20	$7^-/8^+$	14.2±0.4/16.3±0.4		
23.01	346±27	8^+	15.8±0.9		

TABLE II. Table detailing the centroids and Full-Width-at-Half-Maximum of the states observed in the reaction ^{12}C(^{16}O,^{20}Ne α)α at E$_{c.m}$ = 27.0 MeV. The ^{20}Ne and α are detected in coincidence in the hybrid and PSSD4, respectively. In reference [26], only those states observed through an identical entrance and exit channel to the present work have been considered.

E_{ex} $\pm$	FWHM	J^{π}	l_i	ref. [26]	
(MeV)	(keV)	($\hbar$)	($\hbar$)	E_{ex} (MeV)	J^{π} ($\hbar$)
				16.46	7^-
16.52	235$\pm$10	6^+	16.47$\pm$0.65	16.55	8^++9^-
				16.59	6^+
				16.84	8^+
				16.86	6^+
				17.60	(6^+)
17.96	202$\pm$29			17.9	(4^++6^+)
18.71	328$\pm$141				
19.58	241$\pm$31				
20.44	294$\pm$44				
21.16	289$\pm$76				
21.71	293$\pm$94				
22.39	250$\pm$41				
23.06	365$\pm$25	8^+	15.89$\pm$0.15		

figure 1, Kelly et al.

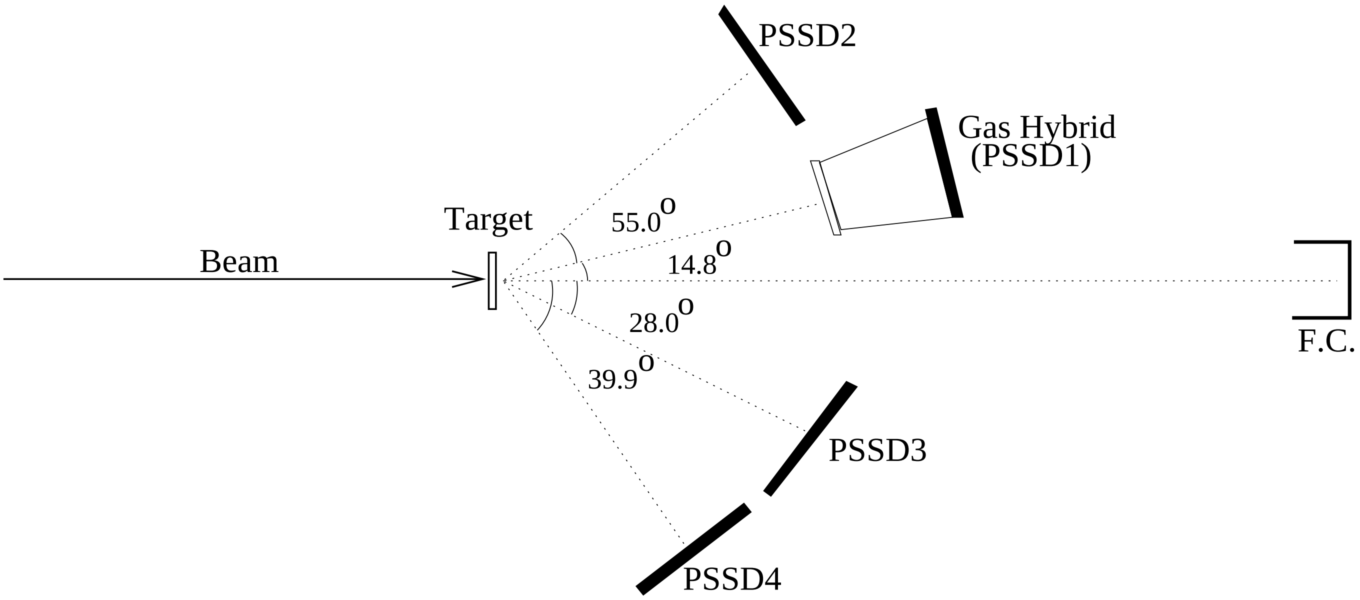

figure 2, Kelly et al.

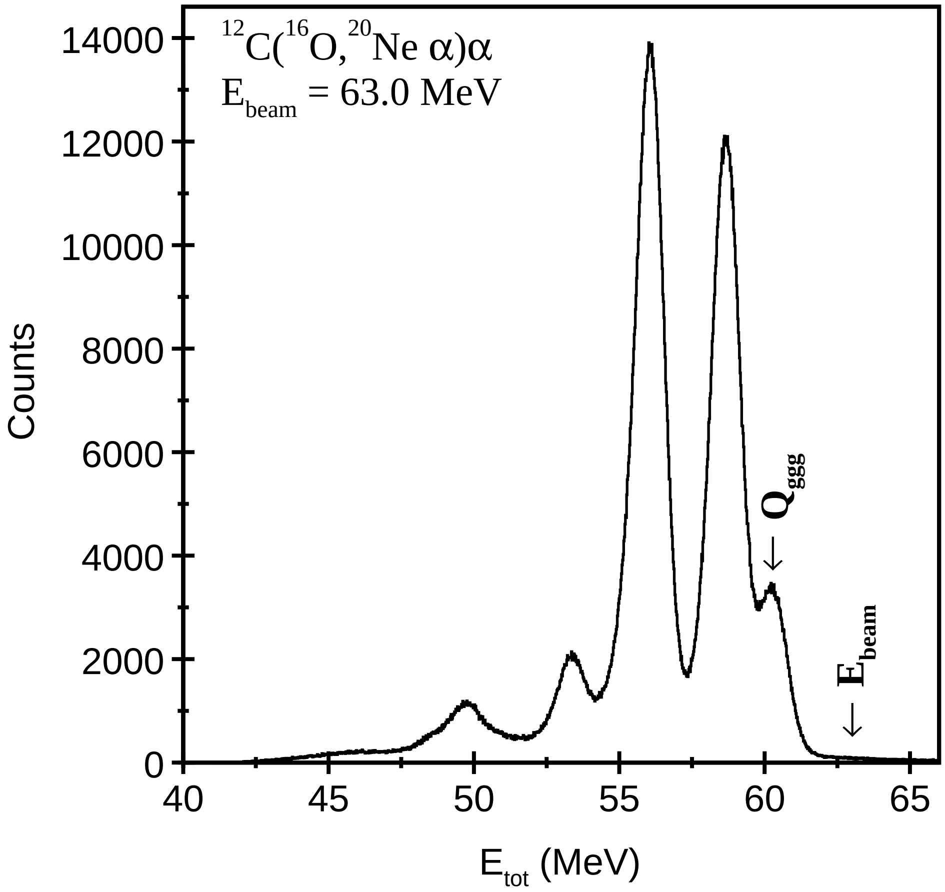

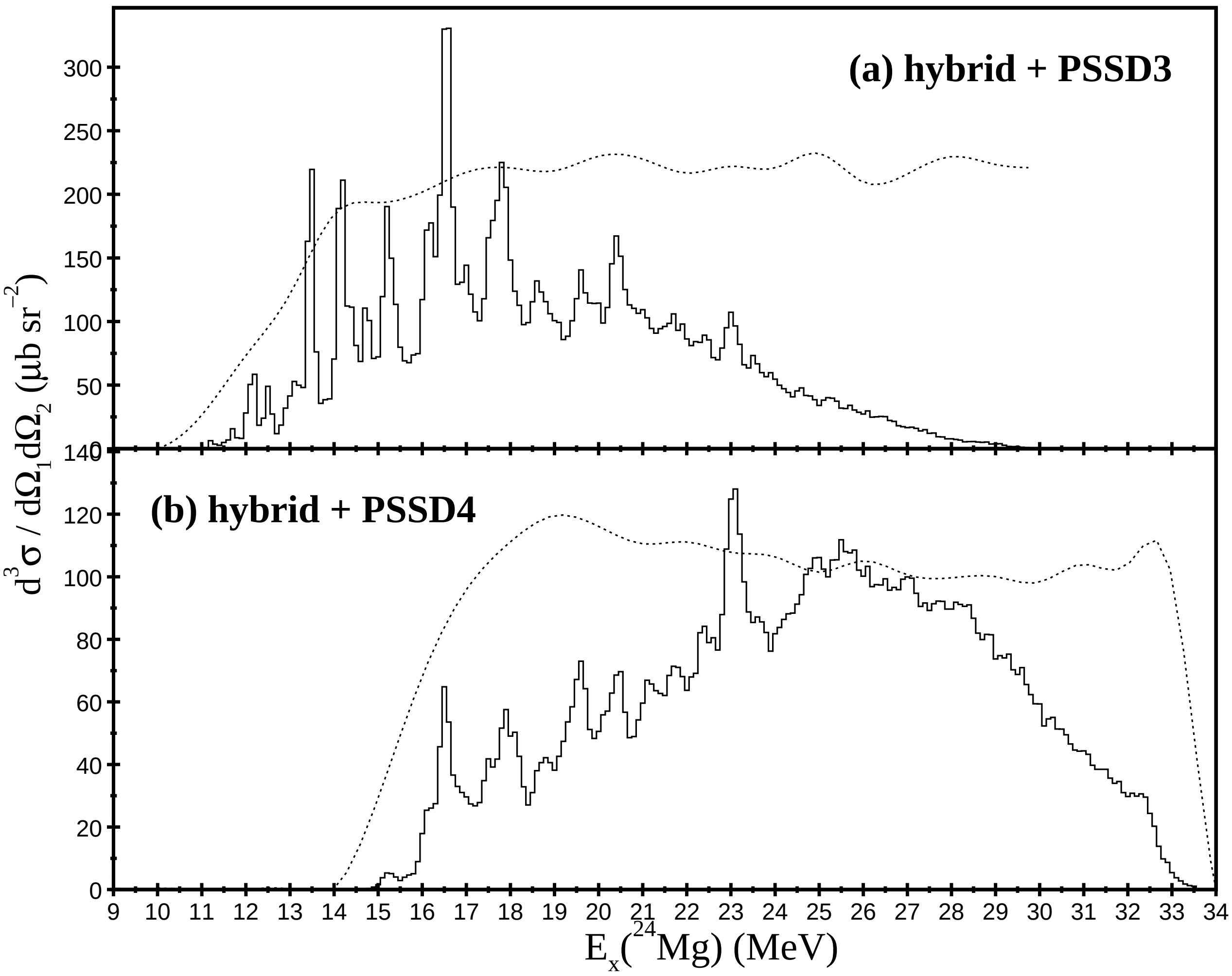

figure 3, Kelly et al.

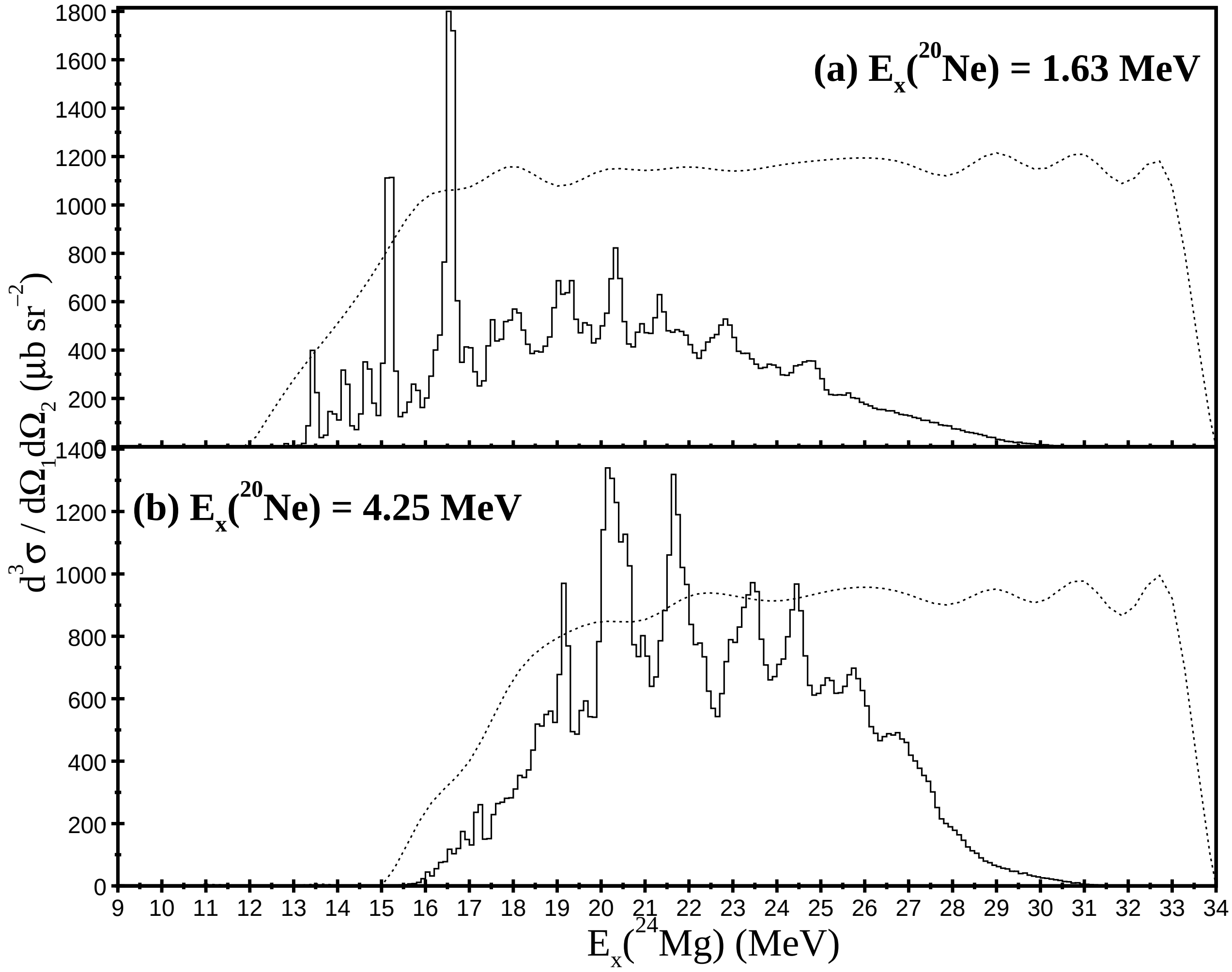

figure 4, Kelly et al.

figure 5, Kelly et al.

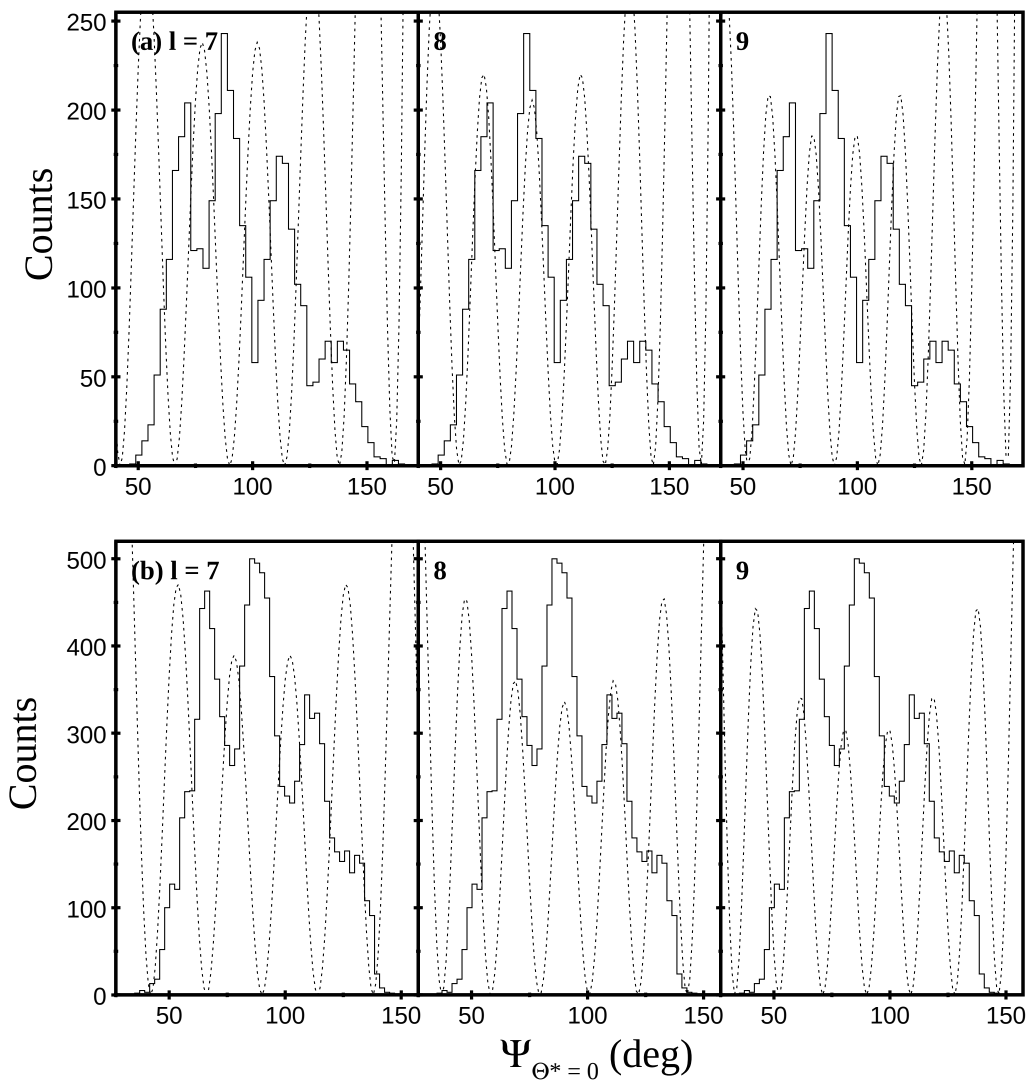

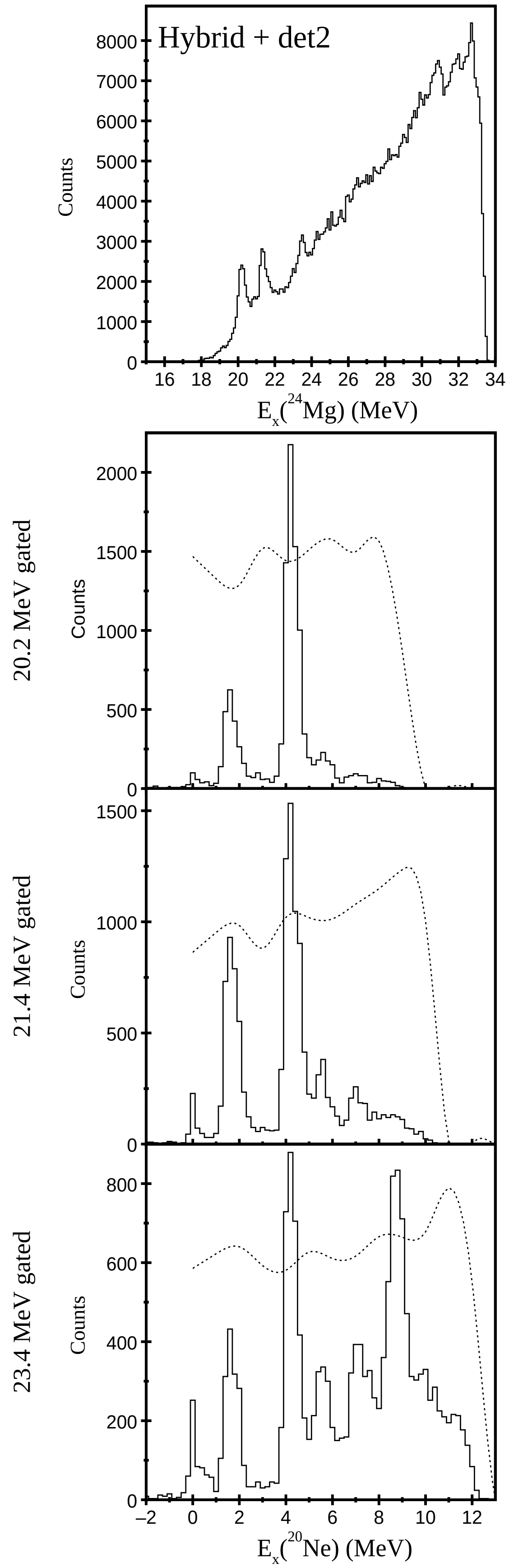

figure 6
Kelly et al.

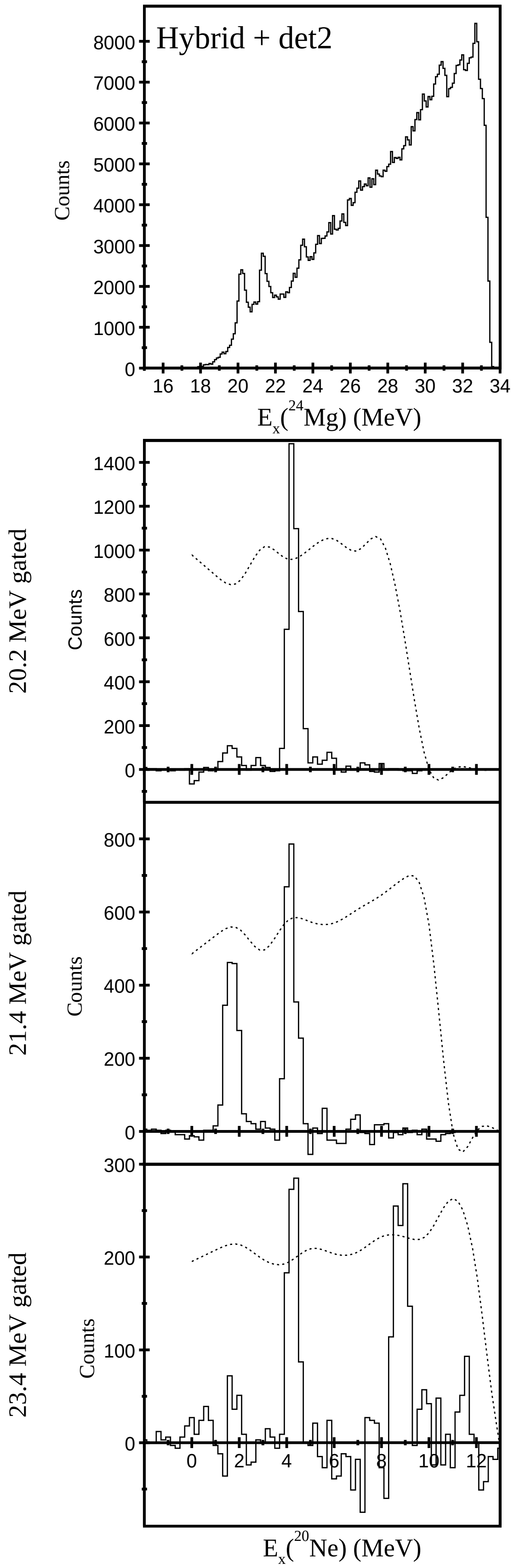

figure 7
Kelly et al.

figure 8, Kelly et al.

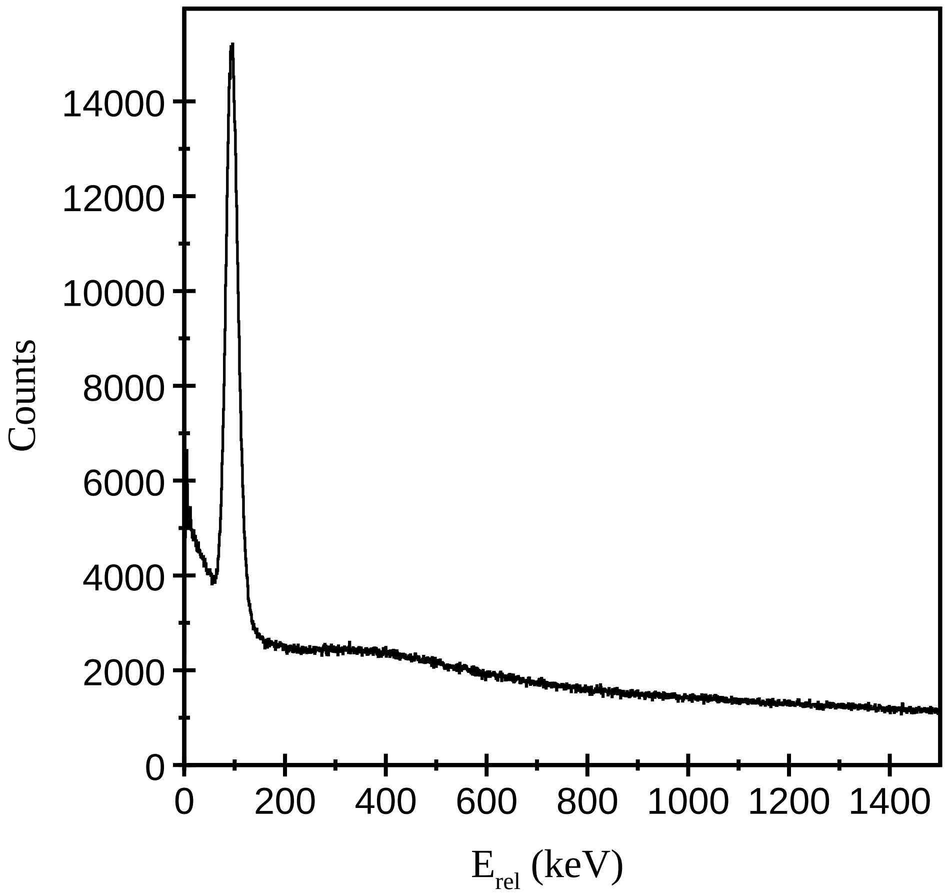

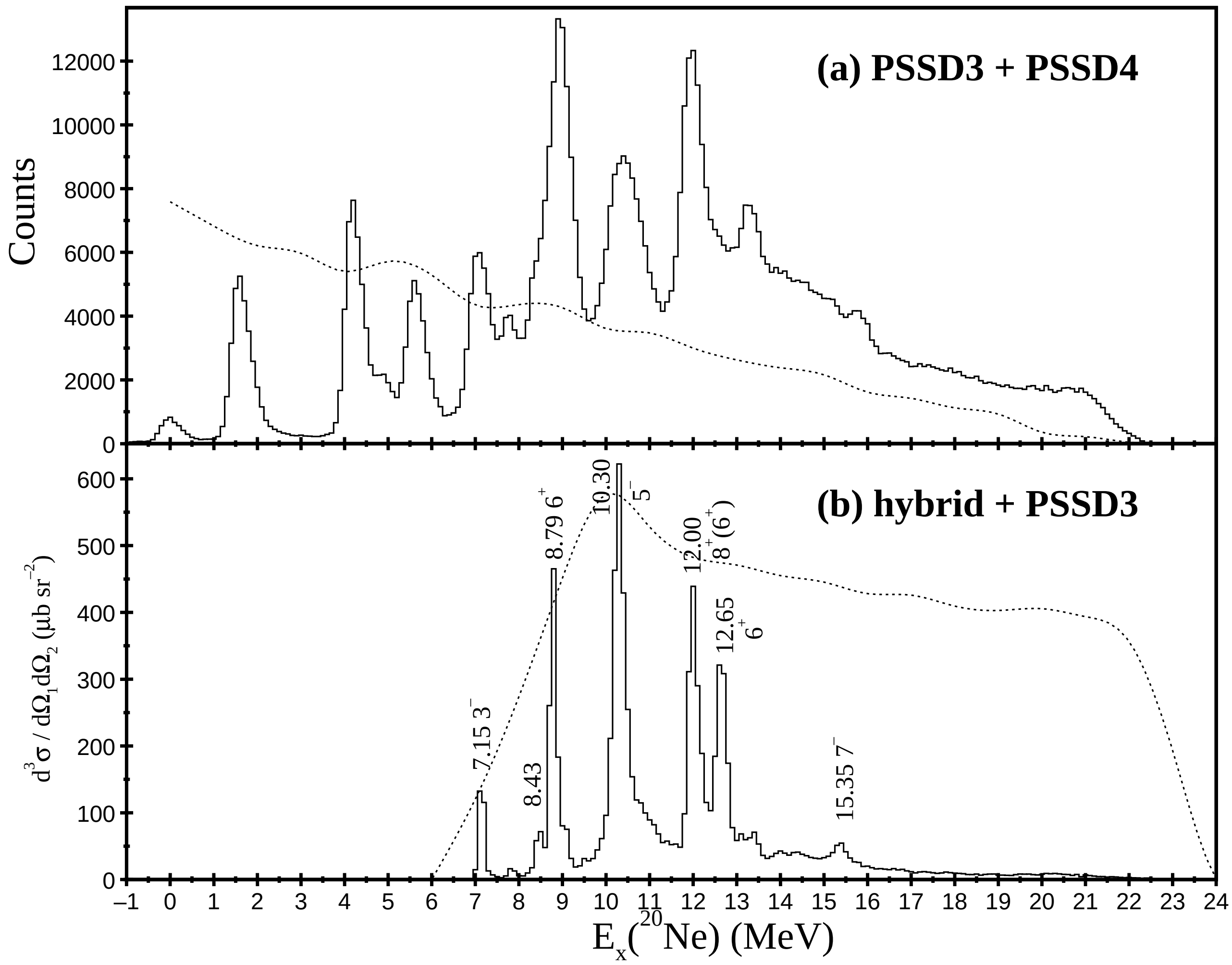

figure 9, Kelly et al.